

Fast Regeneration of CdSe Quantum Dots by Ru Dye in Sensitized TiO₂ Electrodes

Iván Mora-Seró,^{*,†} Vlassis Likodimos,[‡] Sixto Giménez,[†] Eugenia Martínez-Ferrero,[§]
Josep Albero,[§] Emilio Palomares,^{*,§,||} Athanassios G. Kontos,[‡] Polycarpus Falaras,^{*,‡} and
Juan Bisquert[†]

Grup de dispositius Fotovoltaics i Optoelectrònics, Departament de Física, Universitat Jaume I, 12071 Castelló, Spain, Institute of Physical Chemistry, NSCR “Demokritos”, 15310 Aghia Paraskevi Attikis, Athens, Greece, Institute of Chemical Research of Catalonia (ICIQ), Avda. Països Catalans 16, 43007 Tarragona, Spain, and ICREA, Avda. Lluís Companys 28, Barcelona 08020, Barcelona, Spain

Received: January 21, 2010; Revised Manuscript Received: March 2, 2010

Interacting properties of colloidal CdSe quantum dots (QDs) and polypyridyl ruthenium dyes employed as cosensitizers of mesoporous TiO₂ electrodes as well as the effect of QDs coating and anchoring mode (direct and linker adsorption) have been investigated by photoluminescence (PL), Raman, and transient absorption (TAS) spectroscopies. Direct adsorption of QDs on TiO₂ leads to a more efficient PL quenching compared to that of QDs attached by means of a molecular linker (cysteine). This fact suggests higher electron injection for the former anchoring mode. Coating of ZnS on CdSe QDs sensitized TiO₂ electrodes passivates the QDs surface states and partially releases quantum confinement effects, as is observed in colloidal core–shell nanoparticles. Subsequent cosensitization with a ruthenium molecular dye dramatically quenches the PL of the QDs/TiO₂ electrodes, even in the presence of ZnS coating, indicating the presence of strong photoinduced charge transfer between the CdSe QDs and the dye molecules. This is firmly supported by TAS spectroscopy on the interfacial recombination kinetics that points to the fast hole transfer from the photoexcited QDs to the dye. The regenerating action of molecular dyes for QD sensitizers can have important implications in the development of efficient photovoltaic devices based on the synergistic action of dye-QD-TiO₂ heterostructures.

Introduction

Semiconductor materials constitute the basis of photovoltaic devices governing the solar energy-to-electricity conversion field. When these materials are scaled down to the nanometer range, new and fascinating properties appear, distinctly different from their bulk counterparts, as a consequence of the effect of quantum confinement. Yet, some of their bulk properties, which are key for efficient light-to-energy conversion devices as, for example, the high extinction coefficient¹ and the large intrinsic dipole moment² are preserved at the nanoscale. In addition, the band gap of semiconductor quantum dots (QDs) can be easily tuned¹ by control of their size and shape, providing a fertile ground for the design of light-absorbing materials with tailored optical properties.

One of the most attractive configurations to exploit the unique light-harvesting capability of QDs spanning the whole visible range is the quantum dot-sensitized solar cell (QDSC),^{3–5} where QDs substitute the molecular dyes in a cell configuration analogous to that of dye-sensitized solar cells.⁶ In particular, colloidal QDs hold great promise as light-absorbing materials with tailored and well-controlled morphological characteristics (shape and size) that can be utilized as sensitizers of wide band gap nanostructured semiconductors (e.g., TiO₂, ZnO).^{7–12} Recent studies have shown that preformed colloidal QDs can be adsorbed onto TiO₂ photoelectrodes by *linker adsorption* (LA), realized through bifunctional linker molecules,^{9–12} as well as

direct adsorption (DA), where QDs dispersed in appropriate organic media can be successfully tethered onto TiO₂ without any mediating linker.^{7,8} However, it is important to note that the exact effect of the adsorption method on the performance of QDSCs is a topic that only recently has started to be investigated.^{13–15}

One of the most striking properties imparted on QDs by quantum confinement is their highly efficient and tunable photoluminescence (PL) that together with the low-cost processing of colloidal synthesis¹⁶ threads most practical applications currently pursued for colloidal QDs, ranging from light-emitting diodes¹⁷ to fluorescent labels for biological imaging.¹⁸ However, the utilization of colloidal semiconductor nanocrystals as sensitizers in QDSCs implies efficient charge transfer to the wide band gap semiconductor electrode that renders internal radiative recombination and the concomitant PL emission, detrimental for such devices. Anchoring of CdSe QDs onto TiO₂ leads to significant quenching of their emission,¹⁹ due to the injection of photogenerated electrons into the TiO₂ conduction band (CB). In that case, steady state as well as transient PL measurements can be fruitfully applied to quantify charge transfer kinetics from QDs of different sizes to TiO₂²⁰ as well as to trace the influence of the adsorption method.²¹ Furthermore, PL measurements can be used to elucidate the interactions of QDs with other materials used for cosensitizing or coating purposes such as molecular dyes and ZnS. In fact, it has been shown that ZnS coating of CdSe QDs leads to an almost doubled photocurrent in QDSCs.^{7,22}

On the other hand, combination of QDs and molecular dyes provides a particularly powerful route to create novel composite heterostructures with enhanced light harvesting ability. In this sense, colloidal QDs may serve as an excellent component for

* To whom correspondence should be addressed. E-mail: sero@fca.uji.es, epalomares@iciq.es, and papi@chem.demokritos.gr.

[†] Universitat Jaume I.

[‡] Institute of Physical Chemistry.

[§] Institute of Chemical Research of Catalonia.

^{||} ICREA, Avda. Lluís Companys.

the development of more sophisticated heterostructures such as supracollector nanocomposites, exploiting the charge transfer interaction between semiconductor QDs and molecular dyes. The main purpose is to augment the spectral absorption range in QDSCs and to reduce the internal recombination of QDs.^{23,24} In that case, fast scavenging of photogenerated holes in QD sensitizers by a molecular dye can outbalance the competition between electron transfer from QDs to TiO₂ and the internal relaxation of the QD excited state, leading to higher electron injection yields.^{25,26} Simultaneously, light absorption can be drastically enhanced over a broad spectral range better matching the solar irradiance, provided that a suitable combination of QDs and dye complexes with appropriate charge transfer energetics is used.¹⁹

In the present work, the interaction between colloidal CdSe/ZnS-coated QDs and the polypyridyl ruthenium molecular dye N719 has been systematically investigated in cosensitized mesoporous TiO₂ layers for both modes of attachment (DA and LA), employing PL emission and resonance Raman measurements. These techniques provide sensitive experimental probes of the individual components and the underlying interfacial interactions in the TiO₂/QD/dye hybrid system. Specifically, resonance Raman spectroscopy has been proved to be a powerful technique to resolve the chemisorption of a single dye monolayer on nanocrystalline TiO₂ films and the coordinative interactions of the individual components in dye-sensitized solar cells^{27–29} as well as optical phonon confinement effects, exciton–phonon coupling, and interfacial stress in colloidal core–shell QDs.^{30,31} Moreover, to shed more light on the origin of the QD–dye coupling, we have investigated the interfacial electron recombination dynamics in the cosensitized TiO₂ by transient absorption spectroscopy (TAS). The ensuing results unveil marked PL quenching upon dye postsensitization of TiO₂/QD electrodes that depends on the specific QDs adsorption mode, revealing that the dye plays a major role on the regeneration of the photooxidized QDs, which turns into higher electron injection into TiO₂.

Experimental Section

Colloidal CdSe QDs capped with trioctylphosphine (TOP) were prepared by a solvothermal route that allows size control³² in a toluene dispersion. Mesoscopic TiO₂ films approximately 10 μm thick were prepared by using a colloidal titania paste with 20–450 nm TiO₂ particle size (Dyesol 18NR-AO) deposited on transparent conducting substrates and sintered at 450 °C for 30 min. Cysteine has been used as a bifunctional linker in LA adsorption following the procedure reported in ref 11. For DA of QDs onto TiO₂ surface, solvent substitution is needed and a CH₂Cl₂ CdSe QDs dispersion was prepared by centrifugation of the toluene colloidal dispersion, and redissolution.⁸ Different QD adsorption times have been used (8, 19, and 72 h) for both LA and DA. Longer adsorption times lead to a higher amount of adsorbed QDs but this has no influence on the qualitative trends discussed below. Some electrodes were coated with ZnS by twice dipping alternately into 0.1 M Zn(CH₃COO)₂ and 0.1 M Na₂S solutions for 1 min/dip, rinsing with Milli-Q ultrapure water between dips.²² Samples with and without ZnS coating were sensitized with the polypyridyl ruthenium complex *cis*-RuL₂(SCN)₂ (L = 2,2′-bipyridyl-4,4′-dicarboxylic acid) (N719) that is commonly used in high-performance dye-sensitized solar cells (DSC), by dipping them overnight in a 3 × 10^{−4} M solution in ethanol.

The optical and vibrational properties of the QD-sensitized TiO₂ films were investigated by diffuse reflectance, photolu-

minescence, and micro-Raman spectroscopy before and after N719 cosensitization. Diffuse reflectance UV–vis measurements were performed on a Hitachi 3010 spectrophotometer equipped with an integrating sphere. Since the sensitized TiO₂ films are opaque, the absorption of the different samples has been extracted from their diffuse reflectance *R* in Kubelka–Munk units as $F(R) = (1 - R)^2/2R$. Micro-Raman and PL measurements were carried out in backscattering configuration on a Renishaw inVia Reflex spectrometer equipped with a high-sensitivity, deep-depletion CCD detector. The green line of an Ar⁺ ion laser ($\lambda = 514.5$ nm) approaching closely both the metal-to-ligand charge transfer (MLCT) transition of the N719 molecular dye (535 nm)³³ and the first exciton absorption peak of the colloidal CdSe QDs (~540 nm) was used as excitation source for both resonance Raman and PL measurements. The spectra were acquired over the spectral range of 100–3500 cm^{−1} in a single scan (SynchroScan mode). The laser beam was focused on the sample surface using the × 5 and × 50 objectives of a Leica DMLM microscope at a wide range of laser powers regulated by motorized neutral density filters of variable optical density, in order to obtain the optimum S/N ratio for the PL and Raman signals and avoid laser heating. Subtraction of the intense PL background in the Raman spectra has been performed by polynomial fitting and/or cubic spline interpolation routines, while spectral deconvolution has been carried out by nonlinear least-squares fitting of the Raman peaks to a mixed Lorentzian/Gaussian line shape providing the peak position, full width at half-maximum (fwhm), height, and integrated intensity *I* for each Raman band. Resonance Raman has been used to selectively enhance the Raman signal of the semiconductor quantum dots (the excitation wavelength is centered at 514.5 nm, very close to the CdSe QD first excitonic peak, as commented before). Work under nonresonance conditions does not permit the detection of the QD vibration modes, due to their relatively low amount on the TiO₂ matrix. In fact, Raman measurements on the QD-sensitized electrodes under nonresonant excitation conditions (using a near-infrared laser line at 785 nm) show only the anatase TiO₂ Raman modes, whereas the CdSe LO phonon mode could not be traced.

Photophysical characterization was carried out by means of transient absorbance spectroscopy (TAS) measurements on Black Dye/QD-sensitized transparent 4 μm thick TiO₂ films (Black Dye (BD):tris(isothiocyanato)ruthenium(II)-2,2′:6′,2′′-terpyridine-4,4′,4′′-tricarboxylic acid, tris-tetrabutylammonium salt). We used as a blank transparent BD/QD-sensitized ZrO₂ films since the conduction band edge of the inorganic metal oxide is higher than the CB of both CdSe QDs and the BD, and thus, electron injection is avoided. TAS measurements were performed by excitation of the sensitized films at 440 or 640 nm with pulses from a nitrogen-pumped dye laser PTI GL-301 (<1 ns pulse duration, 1 Hz, intensity 0.09 mJ·cm^{−2}). The resulting photoinduced changes in the optical density were monitored at different wavelengths by employing a 150 W tungsten lamp, with 1 nm bandwidth monochromators located before and after the sample, a home-built photodiode based detection system, and a TDS-200 Tektronix oscilloscope.

Results and Discussion

Absorption and Emission Properties. Figure 1 shows the characteristic UV–vis diffuse reflectance spectra in Kubelka–Munk units for the QD-TiO₂ electrodes (DA for 72 h) before and after cosensitization with the N719 dye, compared with the corresponding data for the bare TiO₂ and N719-sensitized TiO₂ films. Adsorption of the CdSe QDs on TiO₂ extends its absorption

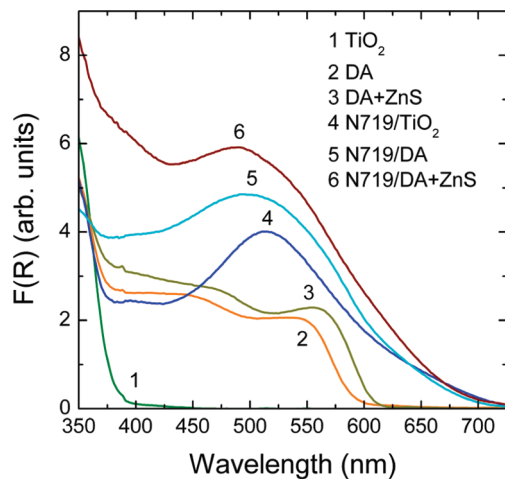


Figure 1. Kubelka–Munk plot of the diffuse reflectance spectra for the TiO₂ films sensitized with DA QDs for 72 h, before and after N719 cosensitization. The corresponding data for bare TiO₂ are included for comparison.

spectrum into the visible region with two pronounced local maxima, a broad one at 445 and a sharper one at 540 nm, reflecting the contributions of the characteristic exciton peaks of the parent colloidal QDs.⁸ Coating with ZnS leads to an increase of the optical absorption and a red-shift of the first absorption exciton peak by approximately 15 nm. The presence of electronic coupling between ZnS and the CdSe QDs can be accordingly inferred, similar to core–shell CdSe/ZnS nanocrystals,³⁴ where tunneling of the QD electron wave function into the surrounding ZnS shell reduces the confinement energy and causes the shift of the exciton peaks to lower energies. Postsensitization with the N719 molecular dye leads to a significant increase of the optical absorption in the visible range, encompassing both the fine structure of the QD absorption, which eventually becomes smeared out, and the prominent contribution of the N719 metal-to-ligand charge transfer (MLCT) transition (Figure 1). Analogous behavior has been observed for the samples sensitized with LA QDs.

A much more pronounced effect is evidenced though in the variation of the PL emission spectra after dye cosensitization of the QD/TiO₂ electrodes. Figure 2a compares the PL spectra of the QD-sensitized electrodes (DA and LA), where the PL amplitude has been normalized to the total amount of adsorbed QDs by using the corresponding values of the first QD absorption maximum. All the QD/TiO₂ samples exhibit the sharp PL peaks stemming from the band-edge emission of CdSe QDs. A difference of about 15 nm is observed in the PL peak position between the LA (575 nm) and DA (590 nm) modes, arising from the variation of the corresponding spectra for the parent colloidal dispersions,⁸ while ZnS deposition leads to a red-shift of the emission peak, correlating with the variation of the corresponding absorption measurements, see Figure 1.

Figure 2b shows the evolution of the normalized photoluminescence peak intensity PL_{norm} with the QD adsorption time for the DA and LA modes. In that case, two general trends can be identified: (i) a systematic increase of PL for the ZnS-coated QD/TiO₂ electrodes for both adsorption modes and (ii) a higher PL intensity for the LA samples in comparison with the DA ones. The former effect indicates a passivation of the CdSe QDs by the ZnS coating, increasing the luminescent quantum yield. Very recently, we have shown that the main effect of the ZnS coating on the QDSCs performance is a dramatic reduction of the recombination of photoinjected electrons in TiO₂ with the

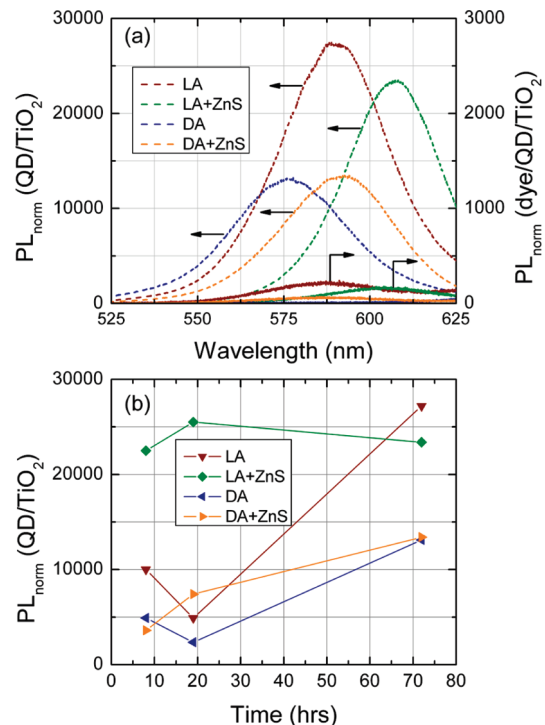


Figure 2. Photoluminescence emission spectra for the sensitized electrodes (DA and LA), normalized to the absorption values of the first QD excitonic peak. (a) PL_{norm} for QD sensitized samples before (QD/TiO₂, dashed line) and after (dye/QD/TiO₂, solid line) N719 dye adsorption. QD adsorption time: 72 h. (b) PL_{norm} intensity for the QD/TiO₂ samples with and without ZnS coating, as a function the QD adsorption time.

redox couple in the electrolyte by the interposition of the ZnS intermediate layer.¹⁵ In addition, both the red shift and the enhancement of the optical absorption and the PL intensity caused by ZnS coating are consistent with the corresponding variations on CdSe/ZnS core–shell nanoparticles, where the ZnS shell improves the PL quantum yield of the CdSe core by passivating the QD surface states.³⁴ Comparing the effect of the adsorption mode on the PL emission, the systematically enhanced PL of the LA samples provides direct evidence for a significantly higher radiative recombination rate due to the presence of the molecular linker, suggesting less efficient QD binding and charge transfer to TiO₂ compared to the DA samples. On the other hand, the absence of a mediating linker in the direct adsorption mode leads to relatively lower PL emission and thus more efficient electron injection from QDs into TiO₂. This result corroborates the higher photovoltaic conversion efficiency reported for colloidal QDSCs, using the DA variant for QD attachment in comparison with the LA.⁷

Most importantly, cosensitization of the QD/TiO₂ samples with the N719 dye leads to a marked reduction of the QD emission, independently of the adsorption mode, as seen in Figure 2a. To quantify this prominent effect, we have calculated the intensity ratio $r_{\text{PL}} = PL_{\text{QD}}/PL_{\text{QD-dye}}$ using the PL intensity before (PL_{QD}) and after ($PL_{\text{QD-dye}}$) postsensitization of the QD/TiO₂ samples with the N719 dye, as shown in Table 1, where the corresponding variation of the optical absorption maxima in Kubelka–Munk units $F(R)$ is also included. Dye adsorption is accordingly found to decrease the QD emission by 2–3 orders of magnitude for all samples, the most pronounced reduction occurring for the uncoated DA samples, where PL emission is nearly totally quenched ($r_{\text{PL}} = 5 \times 10^3$). Explicit comparison between the different types of QD/TiO₂ samples shows that PL

TABLE 1: $F(R)$ Measured from the Kubelka–Munk Plots at 514 nm for the Samples Sensitized with CdSe QDs ($F(R)_{\text{QD}}$) and with QDs + Dye ($F(R)_{\text{dye-QD}}$)^d

	$F(R)_{\text{QD}}$	$F(R)_{\text{dye-QD}}$	$\Delta F(R)^a$	r_{PL}^b	r_{Raman}^c
DA	2.05	5.60	3.55	5000	15
DA-ZnS	2.17	4.76	2.59	220	5
LA	1.84	4.32	2.48	130	6
LA-ZnS	2.42	4.92	2.50	150	8

^a $\Delta F(R) = F(R)_{\text{dye-QD}} - F(R)_{\text{QD}}$. ^b $r_{\text{PL}} = \text{PL}_{\text{QD}}/\text{PL}_{\text{QD-dye}}$ (PL = PL intensity). ^c $r_{\text{Raman}} = I_{\text{LO}}^{\text{QD}}/I_{\text{LO}}^{\text{QD-dye}}$, where $I_{\text{LO}}^{\text{LO}}$ = Raman intensity of the CdSe LO mode. ^d QD adsorption time: 72 h. PL vs Raman intensity reduction ratios after dye absorption at 514 nm.

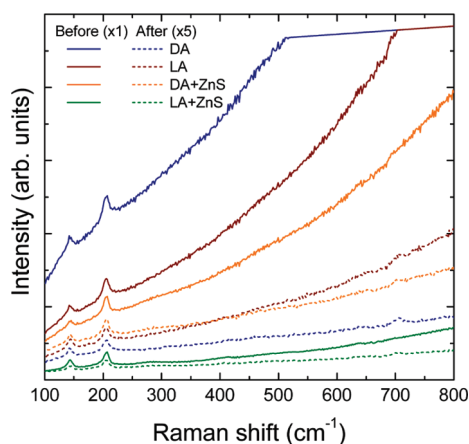


Figure 3. Resonance Raman spectra of the QD/TiO₂ samples before (solid lines) and after (dashed lines) N719 cosensitization, with and without the ZnS coating, at 514.5 nm.

quenching is much higher for the DA than the LA mode for similar values of the optical absorption $F(R)$, while the ZnS shell also reduces the extent of PL quenching for the DA samples. This conspicuous quenching of the CdSe QD emission upon interaction with the Ru-polypyridyl molecular complexes provides the first evidence for the photoinduced charge transfer between the CdSe nanocrystals and the N719 dye, as previously suggested,^{19,24,26} and will be elucidated below by means of transient absorption measurements. It is important to point out that the QD–dye interaction is operative even in the presence of an intervening dielectric layer, as indicated by the significant decrease of the PL intensity for the ZnS-coated samples after cosensitization with the N719 dye.

Micro-Raman Spectroscopy. The effectiveness of the dye postsensitization to quench the QD emission together with the identification of the dye/CdSe + ZnS/TiO₂ components and their electronic coupling has been further explored by micro-Raman spectroscopy. Figure 3 displays the micro-Raman spectra of the QD/TiO₂ samples before and after dye sensitization at 514.5 nm, where the strong interplay of the QDs emission impeding the Raman scattering intensity is clearly evinced. For all QD-sensitized samples, we can identify the most intense E_g Raman mode of anatase TiO₂ at 142 cm⁻¹ and the resonantly excited longitudinal optical (LO) phonon of CdSe QDs at ~205 cm⁻¹ (vide infra) superimposed on the PL background, which, depending on the PL peak position and intensity, severely obstructs the Raman signal. Dye cosensitization reduces drastically the PL background but also the Raman intensity, since the N719 dye absorbs light very efficiently under 514.5 nm excitation that is close to its MLCT transition.³³ In that case, the decrease of the LO Raman intensity, which is directly proportional to the incident light intensity, can be exploited as an independent measure of the light attenuation by the strongly

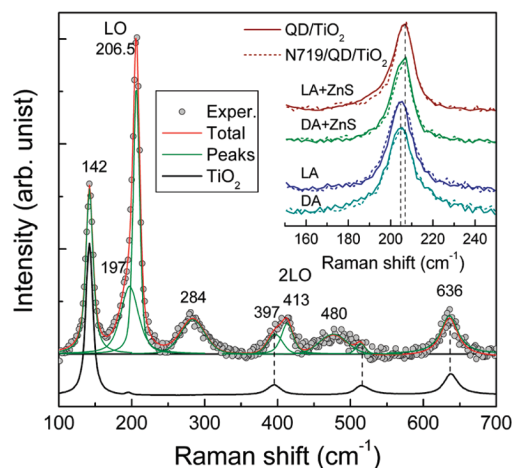


Figure 4. Spectral analysis of the Raman spectrum for the LA-ZnS-sensitized sample at 514.5 nm, in comparison with the bare TiO₂ film. The inset shows the variation of the CdSe LO mode before (solid lines) and after (dashed lines) dye cosensitization.

absorbing dye molecules at 514.5 nm. The corresponding intensity ratios $r_{\text{Raman}} = I_{\text{LO}}^{\text{QD}}/I_{\text{LO}}^{\text{QD-dye}}$, with $I_{\text{LO}}^{\text{LO}}$ being the Raman intensity of the CdSe LO mode, are included in Table 1. These data reveal that in all cases $r_{\text{PL}} \gg r_{\text{Raman}}$, verifying that only a small fraction of the PL quenching could be caused by the effective decrease of the light intensity due to the strong N719 absorption. Moreover, the ratio of r_{PL} to r_{Raman} decreases significantly for the LA samples as well as for the ZnS-coated electrodes, highlighting a clear influence of the attaching mode and the intermediate passivating layer on the dye-QD-TiO₂ coupling. In fact, the large difference between the PL and the Raman signal reduction ratios after dye sensitization reinforces the idea that QDs and dye molecules do not act as independent sensitizers of TiO₂, but rather as a closely coupled system that promotes electron transfer to the semiconducting electrode.¹⁹

Furthermore, Raman spectral analysis allows identifying unambiguously the individual components of the QD-sensitized electrodes and their interactions. Figure 4 shows the deconvoluted Raman spectrum of the LA + ZnS-sensitized sample at 514.5 nm, which exhibits the highest red-shift of the PL background (Figure 2a) and thus the best Raman resolution. The characteristic Raman-active phonons of anatase TiO₂ can be resolved in comparison with the bare TiO₂ electrode, namely the most intense E_g modes at 142 and 636 cm⁻¹ along with the weaker B_{1g} mode at 397 cm⁻¹. The corresponding phonon frequencies are close to those of bulk anatase due to the large particle size in the underlying titania film that hinders phonon confinement effects.²⁷ The most intense Raman peak is though the first-order LO phonon of the CdSe QDs at ~206 cm⁻¹,³¹ due to the resonance Raman effect at 514.5 nm. This was directly confirmed by complementary nonresonant Raman measurements with a near-infrared diode laser at 785 nm as excitation source. In that case, only the anatase modes were observed, while the CdSe LO mode could not be traced, reflecting the much lower amount of QDs relative to that of the TiO₂ film. The CdSe LO mode exhibits the characteristic asymmetric broadening at the low-frequency side stemming from the contribution of confined optical phonons³¹ and/or surface optical (SO) modes.³⁰ Its line shape can be effectively fitted to the superposition of two peaks (Figure 4), the LO mode at 206.5 cm⁻¹ with fwhm of 10 cm⁻¹, reflecting the interplay of phonon confinement and strain in the organic–inorganic interface of colloidal QDs,³⁵ and the low-frequency SO mode at 197 cm⁻¹ with fwhm of 28 cm⁻¹, in good agreement with

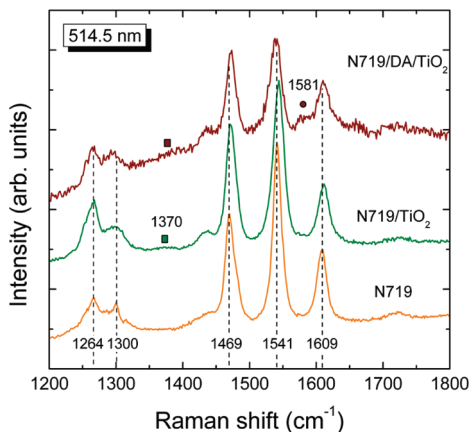


Figure 5. Resonance Raman spectrum of the DA sample after N719 cosensitization in the dye vibration region, compared to N719/TiO₂ and the N719 complex in powder form, at 514.5 nm.

previous results on CdSe/ZnS nanocrystals.^{30,35,36} Comparison of the LO mode before and after N719 dye sensitization (inset of Figure 4) reveals marginal differences between the different sensitized electrodes, indicating that the QDs retain their structural integrity upon dye adsorption. The only systematic variation that is traced concerns a shift of the LO peak from 205 to 206.5 cm⁻¹ together with a decrease of its fwhm from 15 to 10 cm⁻¹ upon deposition of the ZnS coating for both DA and LA samples. This behavior can be attributed to the release of interfacial strain and the passivation of surface defects by the ZnS shell, similar to colloidal CdSe/ZnS QDs.^{30,35} An additional mode is observed at 284 cm⁻¹ together with a rather broad band around 480 cm⁻¹ (Figure 4). These Raman peaks can be attributed to the growth of a mixed CdS_xSe_{1-x} interfacial layer between CdSe QDs and the ZnS shell that gives rise to a CdS-like LO mode at LO_{CdS} ~ 280 cm⁻¹ and its combination with the CdSe LO phonon at LO_{CdSe} + LO_{CdS} ~ 470–490 cm⁻¹, respectively.^{36,37} Moreover, resonant excitation allows identifying the first CdSe overtone 2LO at 413 cm⁻¹, whose integrated intensity ratio to the one-phonon LO mode is a sensitive probe of the exciton–phonon coupling strength.³⁸ The value of I_{2LO}/I_{LO} is determined to be 0.11(1) for the LA + ZnS sample, which is comparable, though smaller than those of CdSe nanocrystals with mean diameter in the range of 2–3 nm.³⁸ This implies weakening of the exciton–phonon interaction upon deposition of the ZnS coating, in good agreement with recent Raman results on CdSe/ZnS nanorods.³⁹

On the other hand, cosensitization of the QD/TiO₂ photoelectrode with the N719 dye leads to distinct variations of the resonance Raman spectrum compared to that of the free dye molecules (Figure 5). The most intense bipyridine ring stretching modes (1470–1615 cm⁻¹) as well as the C–C inter-ring and C–O stretching modes (1250–1320 cm⁻¹) of the N719 dye exhibit clear frequency shifts, intensity variations, and severe broadening upon sensitization of the QD/TiO₂ electrode, exceeding in most cases those observed in the bare N719/TiO₂. This behavior, especially the increased damping of the dye vibrations inferred from the Raman peak broadening, is a characteristic feature of the efficient grafting of the dye molecules on the QD/TiO₂ surface.^{27,28} Furthermore, a weak and broad band appears at about 1370 cm⁻¹ on both N719/TiO₂ and N719/QD/TiO₂ electrodes accompanied by a weak shoulder at ~1580 cm⁻¹ on the QD/TiO₂ electrode. Similar bands have been previously reported in the surface-enhanced Raman spectra of water and ethanol solutions of N719 mixed with silver colloids and were identified with the symmetric and asymmetric COO⁻

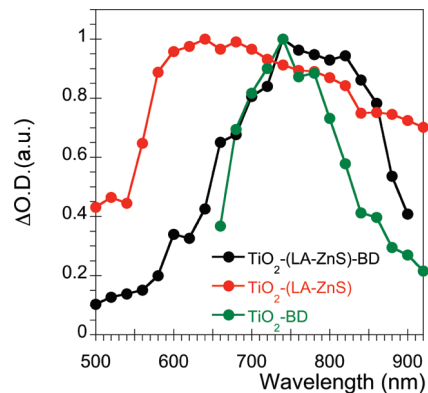


Figure 6. Transient absorption spectra recorded at 100 μs after excitation at $\lambda_{exc} = 440$ nm for TiO₂-(LA-ZnS) and TiO₂-(LA-ZnS)-BD samples, and at $\lambda_{exc} = 640$ nm for the TiO₂-BD sample. The increment in the optical density for the three samples has been normalized to unity for comparison purposes. DA samples present an analogous behavior.

stretching modes, respectively.⁴⁰ The persistence of these modes in the Raman spectra of N719/QD/TiO₂ suggests that the dye complex may be bound onto the CdSe QDs through its carboxylate groups, similar to colloidal metallic nanoparticles.

Transient Absorption Spectroscopy. To establish the relationship between QD and the dye we have undertaken TAS measurements on the TiO₂-QD-BD heterostructured system. The use of BD instead of N719 allows the selective excitation of the dye, for example, at 640 nm, where the QD does not absorb, see Figure 1. On the other hand, it has been previously reported that N719 and BD molecular complexes exhibit similar behavior upon conjugation on QD-sensitized TiO₂ electrodes.¹⁹ Figure 6 shows the normalized spectral transient absorption of QD, BD, and BD-QD-TiO₂ samples at 100 μs after sample excitation. After light excitation at $\lambda_{exc} = 440$ nm QDs are excited. Probing the sample absorption at different wavelengths, λ_{probe} , the spectral pattern of the analyzed samples is obtained by detecting the absorption signal from the QD⁺ cation¹⁴ and the BD⁺ cation. These cations originate from the charge transfer processes between the excited light-absorbers and TiO₂ or between the different light-absorbers. We would also like to notice that from $\lambda_{probe} = 850$ nm to the maximum wavelength of our system (980 nm) the transient absorption spectrum may also have a component due to the absorption of the electrons at the TiO₂ semiconductor film.

The back electron transfer decays from TiO₂ to the oxidized QDs were recorded by measuring exciting at $\lambda_{exc} = 440$ nm and monitoring at $\lambda_{probe} = 620$ nm, the wavelength of maximum absorbance of QD⁺, see Figure 6. Moreover, TAS measurements for BD-QD-TiO₂ for LA and DA samples are shown in Figure 7. When the samples are excited at $\lambda_{exc} = 640$ nm, only the dye is excited. The origin of the cation absorption decay is the recombination of an injected photogenerated electron into TiO₂ with the remaining hole in the cation. In all cases, the recombination decay kinetics expands from nanoseconds to milliseconds time scale and can be fitted by a stretch exponential of the form $\Delta OD = OD_0 \exp(-t/\tau)^\beta$, where OD is the optical density, τ is a characteristic lifetime, and β is the exponential factor. It is also worth noting that the decay on the dye-sensitized DA sample is twice that on the dye-LA suggesting lower recombination when using this synthetic approach that could partially compensate for the lower injection efficiency observed for the LA samples. On the other hand, the addition of the dye to the QD slows down 10 times this back electron transfer, see

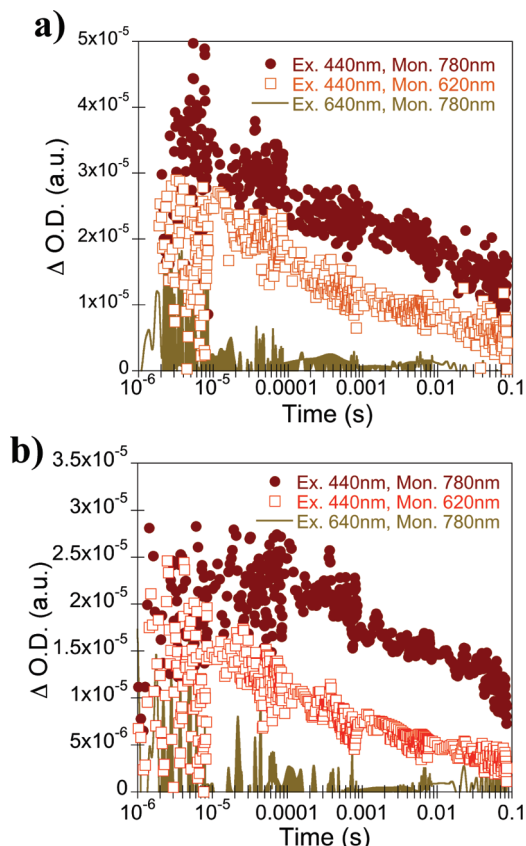


Figure 7. Transient absorption measurements of the TiO₂-QD-dye films excited at $\lambda_{\text{exc}} = 440$ nm, and recorded at $\lambda_{\text{probe}} = 620$ nm (squares) or $\lambda_{\text{probe}} = 780$ nm (full circles), and excited at $\lambda_{\text{exc}} = 640$ nm and probed at $\lambda_{\text{probe}} = 780$ nm (line): (a) LA samples and (b) DA samples.

TABLE 2: Parameters Obtained from the TAS Measurements of Sensitized QD-TiO₂ Electrodes^a

sample	$\lambda_{\text{exc}} - \lambda_{\text{probe}}$	$t_{1/2}$ (ms)	β
TiO ₂ -(LA-ZnS)	440–620	0.54	0.14
TiO ₂ -(LA-ZnS)-BD	440–780	23	0.22
TiO ₂ -(LA-ZnS)-BD	440–620	3.8	0.23
TiO ₂ -(DA-ZnS)	440–620	0.38	0.17
TiO ₂ -(DA-ZnS)-BD	440–780	70	0.42
TiO ₂ -(DA-ZnS)-BD	440–620	1.7	0.32
TiO ₂ -BD	640–760	0.61	0.32

^aBD denotes cosensitization with the black dye. BD-TiO₂ is shown as reference: $t_{1/2}$ is the recombination lifetime deduced from the fwhm of the decay, and β is the exponential factor obtained from the stretched exponential (see text for details).

Table 2, for both deposition methods. To exclude the possibility of electron injection from the black dye directly into TiO₂, the formation of the dye cation has been monitored by excitation at 640 nm and probe at 780 nm. A positive signal is not obtained in any sample suggesting that either there is no formation of BD⁺ or that the recombination kinetics between photoinjected electrons at the QD and the oxidized dye occurs faster than our instrumental response. In any case, the increased recombination lifetime $t_{1/2}$, see Table 2, observed for the QD⁺ after dye attachment can be directly correlated to the influence of the presence of the anchored dye. Finally, the formation of BD⁺ and subsequent regeneration of the QD ground state by the hole transfer from the QD to the anchored dye have been monitored using $\lambda_{\text{exc}} = 440$ nm, where the BD⁺ has no significant absorption, see Figure 6, and monitored the decay at 780 nm. For both DA and LA samples, the resulting decays occur on

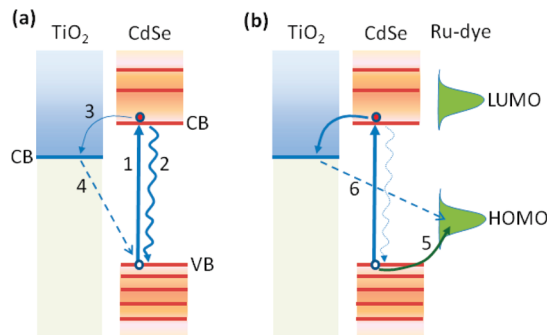


Figure 8. Schematic energy diagram of carrier photogeneration, transfer, and recombination in (a) QD/TiO₂ and (b) dye/QD/TiO₂. Arrows indicate the main processes occurring in sensitized electrodes after light illumination. The thickness of the arrows shows qualitatively the strength of the process. After light illumination electron-hole pairs are photogenerated, process 1. This pair can recombine internally in the QD before any carrier is transferred outside the QD, process 2. This internal recombination can be nonradiative or radiative, the radiative recombination results in the PL signal detected. In addition photogenerated electrons can be transferred to TiO₂, process 3, and they will recombine with the holes left in the QD, process 4. When the dye is attached to the QD the internal recombination, process 2, is strongly reduced (PL quenching), due to the fast hole injection from QD into TiO₂, process 5. In this situation, the recombination of photoinjected electrons in the TiO₂ with photoinjected holes in the dye, process 6, is sensibly slower than the recombination process QD/TiO₂ as has been characterized by TAS measurements.

the same time range, see Figure 7, and are fitted to stretch exponentials. The calculated half-lifetime of BD⁺-QD-TiO₂ is 100 times higher compared to that of BD⁺ anchored onto TiO₂ (Table 2).

The main processes taking place in the sensitized electrodes are indicated in Figure 8. The QD photoexcitation, process 1 in Figure 8a, at $\lambda_{\text{exc}} = 440$ nm promotes the electron injection from the QD excited state to the TiO₂ conduction band, process 3 in Figure 8a, and the immediate regeneration of the QD ground state by the attached dye, process 5 in Figure 8b, which implies that the holes are located at the dyes and the charge recombination process, between the photoinjected electrons at the TiO₂ and the oxidized dyes, process 6 in Figure 8b, is much slower than in the case with no dye attached, process 4 in Figure 8a, due to the increase of distance between the electron donor material and the electron acceptor moiety. The charge recombination dynamics vs distance dependence relationship has already been reported for DSC by Durrant and co-workers.⁴¹

To further confirm our hypothesis we have carried out TAS experiments on ZrO₂ mesoporous films, see Figure 9. The ZrO₂ conduction band edge is much higher in energy than the TiO₂, which prevents the electron injection either from the QD or the dye. Nonetheless, the photoexcitation at 440 nm and probe at 780 nm lead to an extremely fast decay in our micro- to millisecond TAS system, close to the experimental setup response time. This fact indicates that there is an efficient electron transfer from the dye to the QD but the back-electron transfer lifetime occurs faster than microseconds. On the other hand, the fast regeneration of the QD by the Ru dye reduces the internal recombination in QDs, process 2 in Figure 8a, producing the observed quenching in PL. The reduction of internal recombination also increases the amount of injected electrons from QDs into TiO₂, as has been previously observed.^{19,26}

Conclusions

In summary, we have performed a systematic investigation of the electronic coupling between colloidal CdSe QDs and

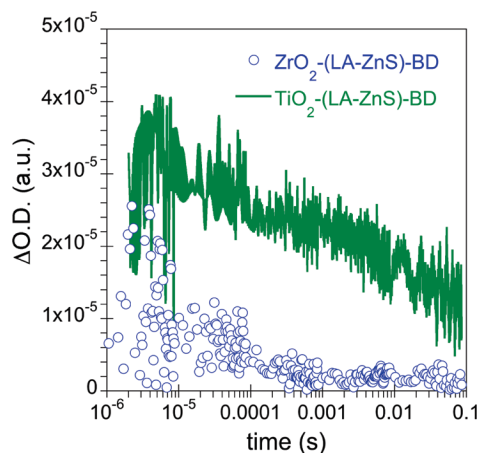


Figure 9. Comparison of the TAS measurements for the TiO₂-(LA-ZnS)-dye and ZrO₂-(LA-ZnS)-dye films excited at $\lambda_{\text{exc}} = 440$ nm and recorded at $\lambda_{\text{probe}} = 780$ nm.

ruthenium molecular dyes used successively as sensitizers of mesoporous TiO₂ films by means of photoluminescence, resonance Raman, and transient absorption spectroscopy, and observed a strong interaction between both of them. Our results indicate the following: (i) Distinct differences in the emission intensity between QDs anchored on TiO₂ electrodes by DA and LA suggest that the absence of a mediating molecular bridge in the former anchoring mode strengthens the coupling and the concomitant electron injection from QDs to TiO₂. (ii) ZnS coating on the QD/TiO₂ electrodes enhances the PL yield acting as a passivation layer of the CdSe QD surface states, as in colloidal core-shell semiconductor nanocrystals. (iii) Most importantly, cosensitization with a ruthenium molecular dye, commonly employed in dye-sensitized solar cells, leads to marked PL quenching, most pronounced in the case of uncoated, directly adsorbed QDs on TiO₂, though clearly sustained even in the presence of ZnS intervening layers. The underlying mechanism is attributed to the fast photoinduced hole transfer from QDs to the dye molecules that act as regenerating agents of the QD sensitizers and promote charge separation in the dye/QD/TiO₂ system. These results could have important implications for the development of QDSC photovoltaic devices exploiting the synergistic function of composite heterostructures consisting of QDs and molecular dyes.

Acknowledgment. This work was partially supported by the Ministerio de Educación y Ciencia of Spain under the project HOPE CSD2007-00007 (Consolider-Ingenio 2010), MAT2007-62982, and by Generalitat Valenciana project PROMETEO/2009/058. S.G., J.A., and E.M.F. acknowledge the Spanish Ministry of Science and Technology for its financial support through the Ramón y Cajal, Torres-Quevedo, and Juan de la Cierva programs, respectively. Prof. Palomares also thanks the ICIQ and ICREA for financial support, and the European Research Council for the ERC fellowship PolyDot. The authors want to acknowledge Dr. Roberto Gómez and his group from University of Alicante (Spain) for providing colloidal QDs.

References and Notes

- (1) Yu, P.; Zhu, K.; Norman, A. G.; Ferrere, S.; Frank, A. J.; Nozik, A. J. *J. Phys. Chem. B* **2006**, *110*, 25451.
- (2) Vogel, R.; Hoyer, P.; Weller, H. *J. Phys. Chem. B* **1994**, *98*, 3183.
- (3) Kamat, P. V. *J. Phys. Chem. C* **2008**, *112*, 18737.
- (4) Klimov, V. I. *J. Phys. Chem. B* **2006**, *110*, 16827.

- (5) Nozik, A. J. *Phys. E (Amsterdam, Neth.)* **2002**, *14*, 115.
- (6) O'Regan, B.; Grätzel, M. *Nature* **1991**, *353*, 737.
- (7) Giménez, S.; Mora-Seró, I.; Macor, L.; Guijarro, N.; Lana-Villarreal, T.; Gómez, R.; Diguna, L. J.; Shen, Q.; Toyoda, T.; Bisquert, J. *Nanotechnology* **2009**, *20*, 295204.
- (8) Guijarro, N.; Lana-Villarreal, T.; Mora-Seró, I.; Bisquert, J.; Gómez, R. *J. Phys. Chem. C* **2009**, *113*, 4208.
- (9) Lee, H. J.; Yum, J.-H.; Leventis, H. C.; Zakeeruddin, S. M.; Haque, S. A.; Chen, P.; Seok, S. I.; Grätzel, M.; Nazeeruddin, M. K. *J. Phys. Chem. C* **2008**, *112*, 11600.
- (10) Leschkie, S. K.; Divakar, R.; Basu, J.; Enache-Pommer, E.; Boecker, J. E.; Carter, C. B.; Kortshagen, U. R.; Norris, D. J.; Aydil, E. S. *Nano Lett.* **2007**, *7*, 1793.
- (11) Mora-Seró, I.; Giménez, S.; Moehl, T.; Fabregat-Santiago, F.; Lana-Villarreal, T.; Gómez, R.; Bisquert, J. *Nanotechnology* **2008**, *19*, 424007.
- (12) Robel, I.; Subramanian, V.; Kuno, M.; Kamat, P. V. *J. Am. Chem. Soc.* **2006**, *128*, 2385.
- (13) Giménez, S.; Lana-Villarreal, T.; Gómez, R.; Agouram, S.; Muñoz-Sanjosé; Mora-Seró, I. 2010. Submitted for publication.
- (14) Martínez-Ferrero, E.; Mora-Seró, I.; Albero, J.; Giménez, S.; Bisquert, J.; Palomares, E. *Phys. Chem. Chem. Phys.* **2010**, *12*, 2819.
- (15) Mora-Seró, I.; Giménez, S.; Fabregat-Santiago, F.; Gómez, R.; Shen, Q.; Toyoda, T.; Bisquert, J. *Acc. Chem. Res.* **2009**, *42*, 1848.
- (16) Yin, Y.; Alivisatos, A. P. *Nature* **2005**, *437*, 664.
- (17) Cho, K.-S.; Lee, E. K.; Joo, W.-J.; Jang, E.; Kim, T.-H.; Lee, S. J.; Kwon, S.-J.; Han, J. Y.; Kim, B.-K.; Choi, B. L.; Kim, J. M. *Nat. Photonics* **2009**, *3*, 341.
- (18) Medintz, I. L.; Uyeda, H. T.; Goldman, E. R.; Mattoussi, H. *Nat. Mater.* **2005**, *4*, 435.
- (19) Mora-Seró, I.; Gross, D.; Mittereder, T.; Lutich, A. A.; Susha, A.; Dittrich, T.; Belaidi, A.; Caballero, R.; Langa, F.; Bisquert, J.; Rogach, A. L. *Small* **2009**, *6*, 221.
- (20) Kongkanand, A.; Tvrdy, K.; Takechi, K.; Kuno, M.; Kamat, P. V. *J. Am. Chem. Soc.* **2008**, *130*, 4007.
- (21) Dibbell, R. S.; Watson, D. F. *J. Phys. Chem. C* **2009**, *113*, 3139.
- (22) Shen, Q.; Kobayashi, J.; Diguna, L. J.; Toyoda, T. *J. Appl. Phys.* **2008**, *103*, 084304.
- (23) Sharma, S. N.; Pillai, Z. S.; Kamat, P. V. *J. Phys. Chem. B* **2003**, *107*, 10088.
- (24) Sykora, M.; Petruska, M. A.; Alstrum-Acevedo, J.; Bezel, I.; Meyer, T. J.; Klimov, V. I. *J. Am. Chem. Soc.* **2006**, *128*, 9984.
- (25) Lee, H. J.; Leventis, H. C.; Moon, S.-J.; Chen, P.; Ito, S.; Haque, S. A.; Torres, T.; Nüesch, F.; Geiger, T.; Zakeeruddin, S. M.; Grätzel, M.; Nazeeruddin, M. K. *Adv. Funct. Mater.* **2009**, *19*, 2735.
- (26) Mora-Seró, I.; Dittrich, T.; Susha, A. S.; Rogach, A. L.; Bisquert, J. *Thin Solid Films* **2008**, *516*, 6994.
- (27) Likodimos, V.; Stergiopoulos, T.; Falaras, P.; Ravi Harikisun, R.; Desilvestro, J.; Tulloch, G. *J. Phys. Chem. C* **2009**, *113*, 9412.
- (28) Pérez León, C.; Kador, L.; Peng, B.; Thelakkat, M. *J. Phys. Chem. B* **2006**, *110*, 8723.
- (29) Stergiopoulos, T.; Bernard, M.-C.; Hugot-Le Goff, A. ç.; Falaras, P. *Coord. Chem. Rev.* **2004**, *248*, 1407.
- (30) Baranov, A. V.; Rakovich, Y. P.; Donegan, J. F.; Perova, T. S.; Moore, R. A.; Talapin, D. V.; Rogach, A. L.; Masumoto, Y.; Nabiev, I. *Phys. Rev. B* **2003**, *68*, 165306.
- (31) Rolo, A. G.; Vasilevskiy, M. I. *J. Raman Spectrosc.* **2007**, *38*, 618.
- (32) Wang, Q.; Pan, D.; Jiang, S.; Ji, X.; An, L.; Jiang, B. *J. Cryst. Growth* **2006**, *286*, 83.
- (33) Nazeeruddin, M. K.; Humphry-Baker, R.; Liska, P.; Grätzel, M. *J. Phys. Chem. B* **2003**, *107*, 8981.
- (34) Dabbousi, B. O.; Rodriguez-Viejo, J.; Mikulec, F. V.; Heine, J. R.; Mattoussi, H.; Ober, R.; Jensen, K. F.; Bawendi, M. G. *J. Phys. Chem. B* **1997**, *101*, 9463.
- (35) Meulenberg, R. W.; Jennings, T.; Strouse, G. F. *Phys. Rev. B* **2004**, *70*, 235311.
- (36) Dzhagan, V. M.; Valakh, M. Y.; Raevskaya, A. E.; Stroyuk, A. L.; Kuchmiy, S. Y.; Zahn, D. R. T. *Nanotechnology* **2007**, *18*, 285701.
- (37) Scamarcio, G.; Spagnolo, V.; Venturi, G.; Lugará, M.; Righini, G. C. *Phys. Rev. B* **1996**, *53*, R10489.
- (38) Alivisatos, A. P.; Harris, T. D.; Carrol, P. J.; Steigerwald, M. L.; Brus, L. E. *J. Chem. Phys.* **1989**, *90*, 3463.
- (39) Lange, H.; Artemyev, M.; Woggon, U.; Niermann, T.; Thomsen, C. *Phys. Rev. B* **2008**, *77*, 193393.
- (40) Pérez León, C.; Kador, L.; Peng, B.; Thelakkat, M. *J. Phys. Chem. B* **2005**, *109*, 5783.
- (41) Clifford, J. N.; Palomares, E.; Nazeeruddin, M. K.; Grätzel, M.; Nelson, J.; Li, X.; Long, N.; Durrant, J. R. *J. Am. Chem. Soc.* **2004**, *126*, 5225.